ACS APPLIED MATERIALS & INTERFACES

Research Article

www.acsami.org

Evaluation of Back Contact in Spray Deposited SnS Thin Film Solar Cells by Impedance Analysis

Malkeshkumar Patel and Abhijit Ray*

School of Solar Energy, Pandit Deendayal Petroleum University, Raisan, Gandhinagar 382007, Gujarat India

Supporting Information

ABSTRACT: The role of back metal (M) contact in sprayed SnS thin film solar cells with a configuration Glass/F:SnO_2/In_2S_3/SnS/M (M = Graphite, Cu, Mo, and Ni) was analyzed and discussed in the present study. Impedance spectroscopy was employed by incorporating constant phase elements (CPE) in the equivalent circuit to investigate the degree of inhomogeneity associated with the heterojunction and M/SnS interfaces. A best fit to Nyquist plot revealed a CPE exponent close to unity for thermally evaporated Cu, making it an ideal back contact. The Bode phase plot also exhibited a higher degree of disorders associated with other M/SnS interfaces. The evaluation scheme is useful for other emerging solar cells developed from low cost processing schemes like spray deposition, spin coating, slurry casting, electrodeposition, etc.

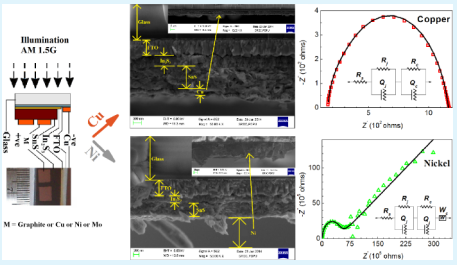

KEYWORDS: *SnS, heterojunction, spray pyrolysis, thin films solar cell, impedance spectroscopy, back metal contacts*

INTRODUCTION

Tin(II) sulfide (SnS) is a p-type semiconductor material with layered structure that crystallizes in orthorhombic unit cells. Due to its direct optical band gap of 1.3 eV, it has a high absorption coefficient (>10^4 cm^{-1}) in the visible range of the solar spectrum and therefore is considered to be the right material for a photovoltaic absorber.[1,2] The SnS materials also enjoy the advantage of fabricating good quality thin films by nonvacuum processes.[2−6] Despite these advantages, SnS thin film solar cells are recorded to have low power conversion efficiency (η). The maximum conversion efficiencies of SnS solar cells recorded to date are 2.1% and 1.32% fabricated by a vacuum[7] and a nonvacuum process,[3,8] respectively. Although, the cells can be fabricated to produce an open circuit voltage as high as 0.7−0.9 V,[9,10] by designing low band-offset n-type heterojunction partners[7] or short circuit current densities of 16−20 mA/cm^2,[1,11] their fill factors are often poor, in the range of 25−40%, due mainly to inhomogeneities and disorders associated with various interfaces. The absorber to metal back contact is one of the major interfaces giving rise to such inhomogeneities and therefore introducing a high series resistance or low shunt resistance in the device. The characterization of defects and inhomogeneities at the p−n interfaces have been studied by several groups using deep level transient spectroscopy (DLTS)[12−14] and thermal admittance spectroscopy (TAS).[15−19] A more convenient technique to characterize the interface defects in terms of their direct effect on the equivalent circuit of the device is the impedance spectroscopy (IS). This technique has drawn great interest not only in fuel cells or corrosion research,[20,21] but also in functional devices, such as solar cells,[22−26] due to its simple measurement procedure, lack of need to heat or cool the samples, high accuracy, and possibility of measurement at large area interfaces. The IS has been widely used to characterize charge transfer and diffusion kinetics in dye sensitized solar cells.[22,23,27] There are also reports to characterize p−n interface in CIGS based solar cells by the IS technique.[28,29] Although, the secondary ion mass spectroscopy (SIMS) has the potential to scan the elements in depth from an interface, the IS in comparison can be used to directly investigate the equivalent circuit elements contributed by various defects, disorders, grain boundaries, elemental diffusion, and inhomogeneities.[30] In the present investigation, we have employed this prevailing IS technique to study the applicability of metal contacts in thin film solar cells as in many cases the metal contacts lead to a lowering of fill factor in the solution processed solar cells. In this work, we report on the fabrication of a Glass/F:SnO_2/In_2S_3/SnS/M (M = Graphite, Cu, Mo, and Ni) heterojunction solar cell, where both the buffer and absorber layers are fabricated by chemical spray pyrolysis (CSP). The back metal options were chosen by virtue of their work function being greater than the electron affinity of SnS to ensure an ohmic contact.[31,32] After initial structural and morphological characterization, the device impedance was measured at different frequencies, and the results were analyzed by incorporating constant phase elements (CPE) in the equivalent circuit to investigate the degree of inhomogeneity associated with each M/SnS interface.

EXPERIMENTAL SECTION

Thin films of SnS and In_2S_3 were prepared by the compressed air assisted CSP technique using aqueous solutions. Tin chloride ($SnCl_2$·

Received: February 19, 2014
Accepted: June 1, 2014
Published: June 1, 2014

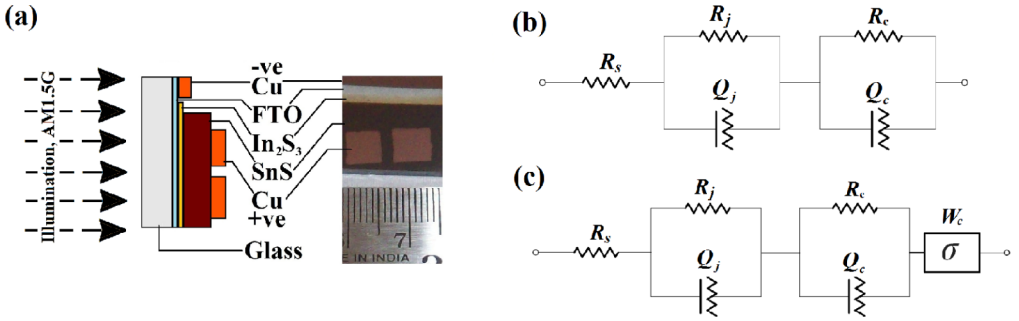

Figure 1. (a) Cross sectional graphics and top view of the developed M/SnS/In_2S_3/F:SnO_2 (here, M = Cu) heterojunction solar cells, (b) and (c) proposed equivalent circuit models of the device for IS applicable to M = Cu and Graphite and M = Ni and Mo, respectively.

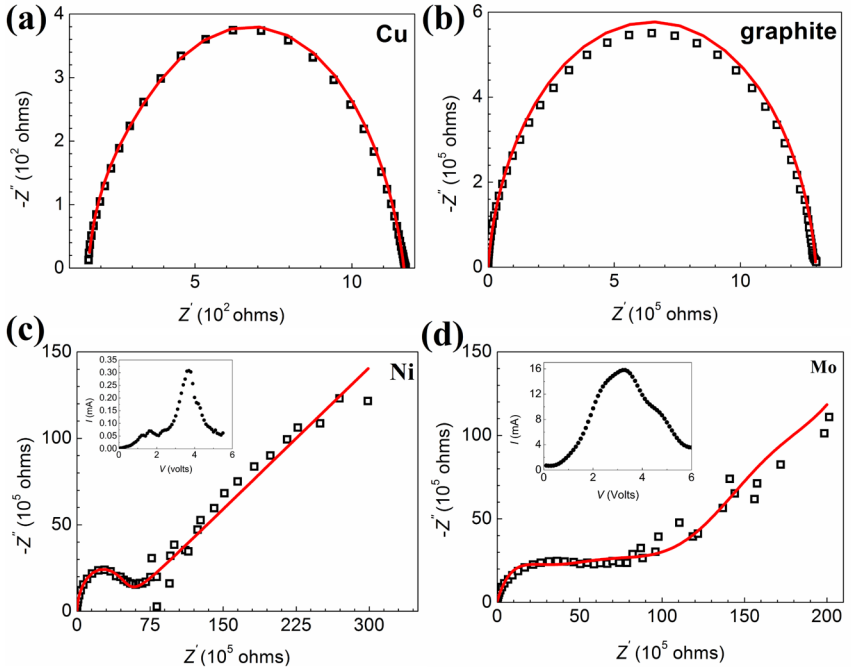

Figure 2. Nyquist plots for M/SnS/In_2S_3/F:SnO_2 devices with various possible back metal (M) contacts (Copper, Graphite, Nickel, And Molybdenum). Solid lines represent fitted curves to an equivalent circuit of the device according to Figure 1(b),(c). Insets are showing the existence of negative resistance in case of Ni and Mo as back contacts, that was not present in the case of Cu and Graphite.

$2H_2O$, >98%, Merck), indium chloride ($InCl_3$, >98%, Sigma) and thiourea (CH_4N_2S, >99%, Merck) were used as precursor sources of Sn, In, and S, respectively. The optimized precursor concentration ratio for SnS and In_2S_3 was fixed at 1:1.5 and 1:6, respectively. The molar optimization scheme for SnS with the help of Photo-electrochemical studies can be found in Suppotrting Information (SI) Figure S4. In_2S_3 was first deposited on ultrasonically cleaned F:SnO_2/Glass substrates (procured from Sigma). An excess concentration of thiourea was taken to compensate for the sulfur loss during the deposition process. For Graphite (PELCO, Product No. 16051) and Ni (PELCO, Product No. 16059), conducting paste of these metals (procured from Ted Pella Inc.) was applied on the SnS by a paint brush, manually. Cu was deposited by thermal evaporation of high purity Cu (99.99%, Alfa Aesar) in a vacuum coater (Hind High Vacuum Co. Ltd., model BC-100) at a set current of 120 A. Mo (purity, 99.99%, Good Fellow) deposition was carried out in a sputter coater (from Milman Thin Films Systems). In all cases, a shadow mask area of 25 mm^2 was used to produce the back contacts. A general architecture of the finished device is shown in Figure 1(a), where the Cu represents one of the back contacts.

The details of structural (X-ray diffraction) and morphological (field emission scanning electron microscopy, FE-SEM) characterization of SnS are found elsewhere[2] and that for In_2S_3 layers are given in the SI. The impedance spectra of the completed device was measured in a potentiostat/galvanostat (Autolab, model PGSTAT302N) attached with a frequency response analysis module (FRA32M). The IS measurement for the developed cells was carried out using an AC signal of amplitude 5 mV in the frequency range from 0.1 Hz to 1 MHz superimposed by a DC bias of 10 mV under actual dark conditions (1 microsun, measured by a solar irradiation meter).

RESULTS AND DISCUSSION

The IS data of Cu and Graphite back contacted devices were analyzed based on the equivalent circuit models, as shown in Figure 1(b). In Figure 1(c), an additional circuit element, σ, the Warburg impedance was required to be included in order to best fit the impedance data of the device with Ni or Mo as back contact. The AC impedance of a given circuit consisting of resistive and reactive elements at an angular frequency ω is given by the following:

$$Z(\omega) = Z'(\omega) + iZ''(\omega) \quad (1)$$

where Z' and Z'' are the real and imaginary part of the impedance, respectively. In the present case, specific to the

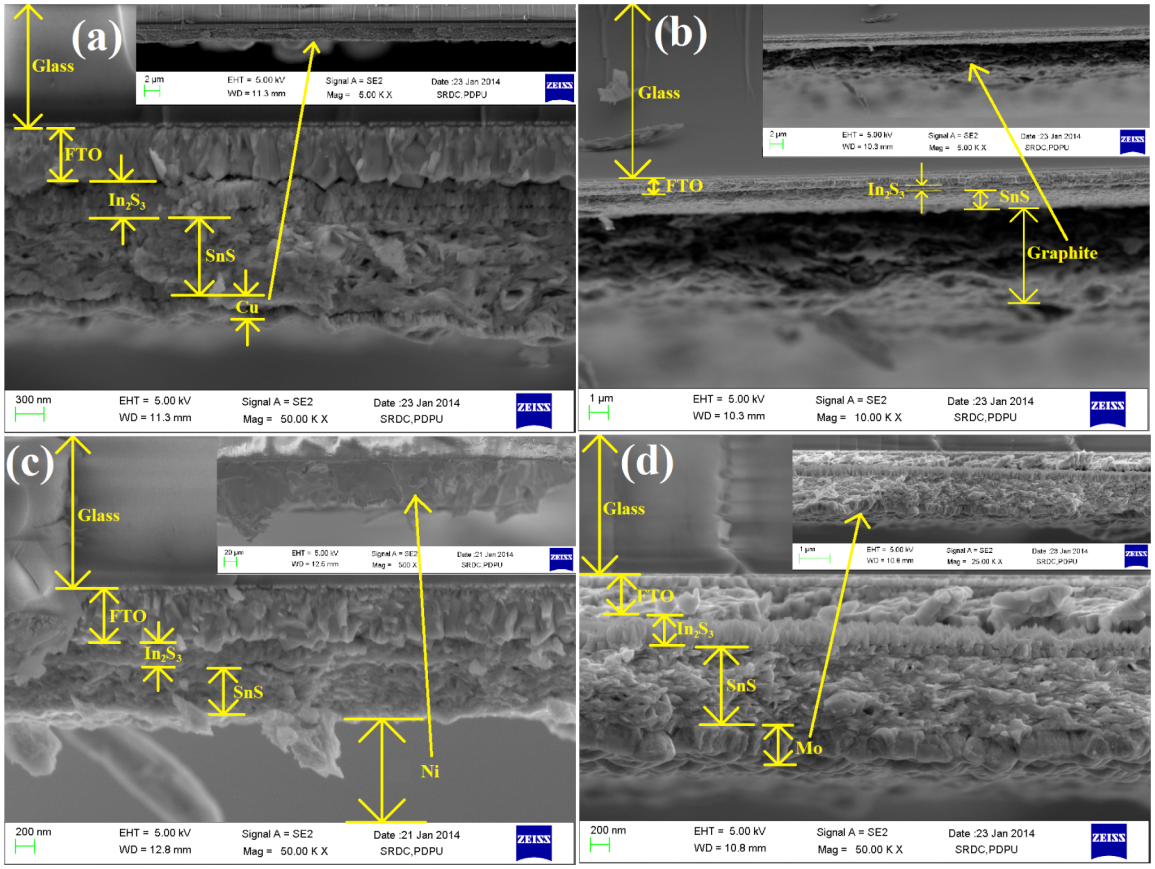

Figure 3. Field emission SEM images of cross section of M/SnS/In_2S_3/F:SnO_2/Glass devices for the back metal, M as (a) Copper, (b) Graphite, (c) Nickel, and (d) Molybdenum. Insets are showing lower magnification images to visualize contact roughness at broader area.

circuit as described in the previous section (as shown in Figure 1(b),(c)), the total impedance can be written as follows:

$$Z(\omega) = R_s + \frac{1}{\frac{1}{R_j} + \frac{1}{Z_{CPE_j}}} + \frac{1}{\frac{1}{R_c} + \frac{1}{Z_{CPE_c}}} \quad (2)$$

for circuit in Figure 1(b),

$$Z(\omega) = R_s + \frac{1}{\frac{1}{R_j} + \frac{1}{Z_{CPE_j}}} + \frac{1}{\frac{1}{R_c} + \frac{1}{Z_{CPE_c}}} + \frac{\sigma}{\sqrt{\omega}}(1 - i) \quad (3)$$

for circuit in Figure 1(c), where, R_s is total series resistance of the device, (R_j, Z_{CPE_j}) and (R_c, Z_{CPE_c}) are the parallel resistance-CPE impedance pair of the p−n junction and back-contact, respectively. The fourth term on the right-hand side of eq 3 represents the Warburg impedance, where σ is the Warburg coefficient. The CPE impedances i.e., Z_{CPE_j} and Z_{CPE_c}, can be defined by their respective CPE exponents (or CPE-n) and frequency independent constant (or CPE-Q) as follows:

$$Z_{CPE} = \frac{1}{(j\omega)^n Q} \quad (4)$$

where, $Z_{CPE} = Z_{CPE_j}$, $Q = Q_j$, $n = n_j$ for the (R_j, Q_j) and $Z_{CPE} = Z_{CPE_c}$, $Q = Q_c$, $n = n_c$ for the (R_c, Q_c) parallel assemblies, respectively.

Figure 2(a)−(d) shows the set of Nyquist plots for thes developed cells. It was noteworthy that both of the cells with Cu and Graphite back contacts (Figure 2(a),(b)) exhibited a semicircle-like Cole−Cole plot, which confirmed the presence of a dominating single space charge region in the hetero-junction, without any other diffusive transport mechanisms. As the impedance spectra are best fit by considering CPE both at the SnS/In_2S_3 and at the M/SnS interfaces, a relative strength of the inhomogeneities around these interfaces can be found from the magnitude of the CPE exponents, n_j and n_c, respectively. The CPE exponent equals to 1, 0, −1 and 0.5, represents the ideal capacitor, resistor, inductor, and Warburg element, respectively. Any values of the CPE exponent between 0 and 1 represent a nonideal capacitor due to defects or roughness at the interface. Typical issues which result in capacitance dispersion as CPE behavior include surface disorder, roughness, varying thickness or composition, nonuniform current distribution, and electrode geometry.[33−35] The measured average surface roughness (R_a) was 52 nm over the length of 200 μm for the sprayed SnS films on the FTO substrate. From the previous study, it has been identified that the R_a of sprayed SnS films varies with the substrate roughness. On the basis of the above observation, a surface roughness is found to be larger when the film is deposited by nonvacuum processes. This nonuniformity of surface roughness can affect the distribution of space charge across the junction, which could be responsible for a capacitance dispersion and the nonideality across the interfaces.

Figure 3 shows SEM images of cross section of the presented devices, where the back contact region is emphasized within the inset. In order to estimate the nonuniformity associated with the metal/semiconductor interface and how it is linked to the resulting impedance spectra, a further image analysis was made

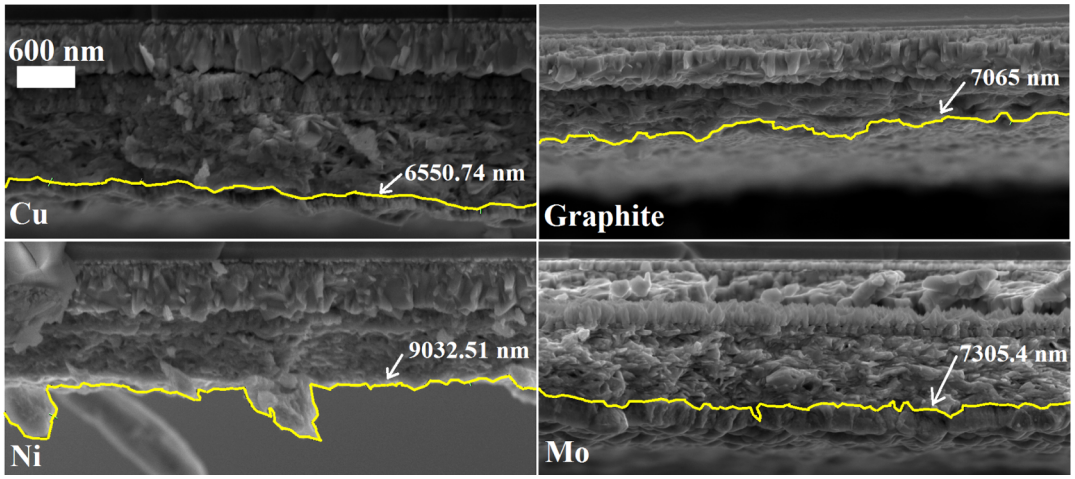

Figure 4. SEM images emphasizing the nonuniformity associated with each of the SnS/M (= Cu, Graphite, Ni, or Mo) interfaces. The highlighted line indicates an envelope over the metal interface.

on the interface of each of the devices. A pixel integrated line profile of these interfaces are shown in Figure 4 with a linear resolution of 5.72 nm. We define an interface nonuniformity index (INI) as,

$$\mathrm{INI} = \frac{L_s}{L_t} \tag{5}$$

where, L_s and L_t are the pixel integrated line length of the actual interface and the straight line length along the horizontal direction, respectively. The estimated values of L_s, L_t, and INI is summarized in Table 1. The largest value of INI = 1.54 was found for Ni, where as it was smallest for Cu.

Table 1. Estimated Values of L_s, L_t, and Interface Non-Uniformity Index (INI) of M/SnS Interfaces from SEM Image Analysis

metal (M)	L_s(nm)	L_t(nm)	INI
Cu	6550.74	5851.43	1.12
Graphite	7065.02	5851.43	1.20
Ni	9032.51	5851.43	1.54
Mo	7305.37	5851.43	1.25

The smallest value of n_c = 0.463 was obtained for Ni back contact, where a substantial nonuniformity of the Ni/SnS interface was demonstrated from the above image analysis. The right-hand cutoff of the spectrum on the real axis in Figure 2 corresponds to the total resistance or low frequency (dc) impedance of the device. A slight deviation into another small semicircle like behavior in the right-most part (low frequency region) of the Cole−Cole plot in Figure 2(b) indicates the presence of a very small time constant, probably due to a weak Schottkey junction behavior of the Graphite back contact. However, this time constant for Graphite was greater than that of Cu, as seen from the imaginary impedance spectra. In this curve, the rising Z'' at low frequency is attributed to capacitance in the circuit, whereas the falling branch is because of associated contact resistance.[36] The time constants of the system consisting of CPEs as listed in Table 2, could be estimated by considering an equivalent capacitance at the junction, C_j^* and at the back contacts, C_{bc}^* using an expression,[37]

$$C^* = \frac{(QR)^{1/n}}{R} \tag{6}$$

where, $C^* = C_j^*$, $R = R_j$, $Q = Q_j$, $n = n_j$ for the (R_j, Q_j) and $C^* = C_{bc}^*$, $R = R_c$, $Q = Q_c$, $n = n_c$ for the (R_c, Q_c) parallel assemblies, respectively.

The time constant calculated by the product of RC^* was an overall value without trying to separate the recombination and diffusion capacitances.[23−25,37−39] Therefore, $\tau_j = R_jC_j^*$ and $\tau_c = R_cC_{bc}^*$ will be referred to simply as the overall time constants of the junction and the back contacts, respectively. The magnitude of the circuit time constants representing the mean relaxation time of the respective interfaces are in good agreement with the reported values in other similar devices.[37] It was further evident from the above calculation that, both cells having Cu and Graphite as back contact show the junction time constant (τ_j) which is about four times larger than that of the back contact (τ_c). In case of Ni and Mo back contacts, the junction time constant, τ_j was found to be of the same order, where as the contact time constant, τ_c was four to six orders larger. For Ni, this may be attributed to the large surface area of Ni electrode in contact with the SnS, as evident from the FE-SEM image in

Table 2. Estimated Fitting Parameters of the Equivalent Circuit for M/SnS/In_2S_3/F:SnO_2 Solar Cell from the Impedance Spectroscopy for Selected Back Metals (M)

		CPE-1 circuit			CPE-2 circuit			time constant		σ
back metal	R_s (Ω)	R_j (Ω)	Q_j (nMho)	n_j	R_c (Ω)	Q_c (nMho)	n_c	τ_j(μs)	τ_c(μs)	(nMho)
Cu	158	960	81.4	0.84	48.8	10.5	0.98	12.8	0.38	
Graphite	158	0.96M	80.0	0.84	49.2k	10.2	1.00	12.9	0.51	
Ni	−6.86k	1.9M	0.013	0.93	9.8M	52.5	0.46	11.9	23 600	159.0
Mo	−7.65k	3.4M	0.06	1.00	4.5M	0.33	0.83	20.0	406	18.0

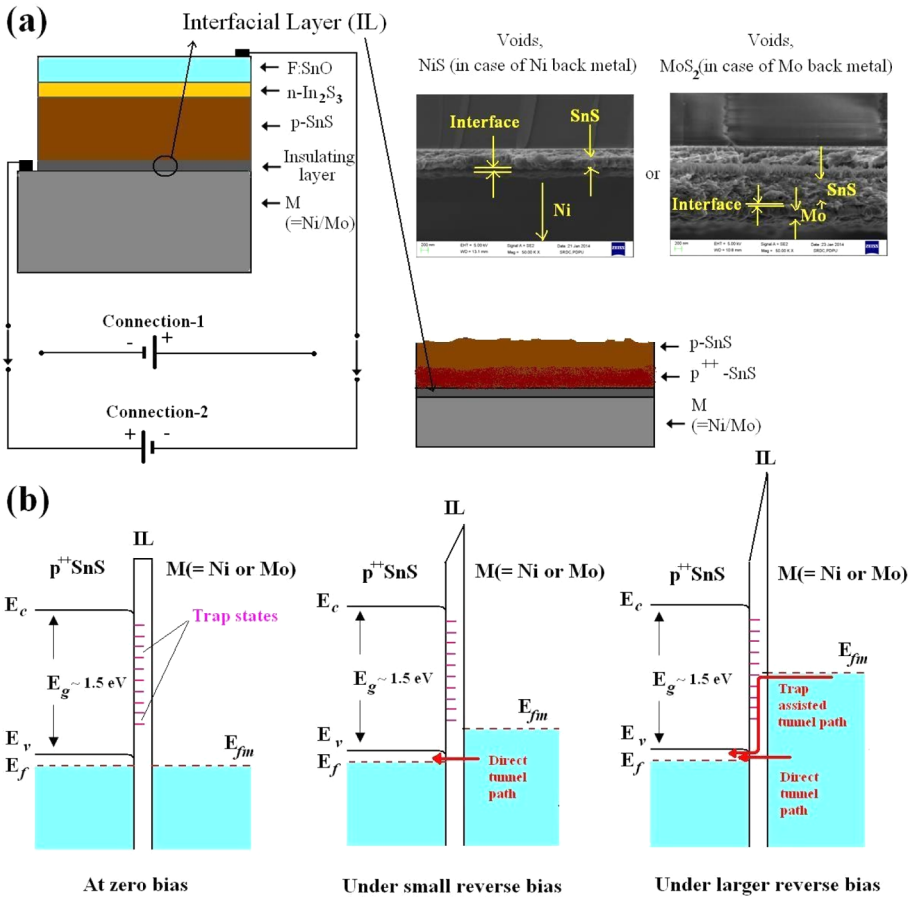

Figure 5. (a) The biasing scheme for the device to test their current–voltage characteristics: Connection-1 represents a reverse biasing to *p*-SnS/*n*-In_2S_3 junction and a forward biasing to M/IL/p^{+2}-SnS tunnel junction, whereas, Connection-2 represents that the M/IL/p^{+2}-SnS tunnel junction is in reverse bias. The interface of the Mo/SnS and Ni/SnS, as shown in the adjacent SEM image, acts as an interfacial layer (IL) to contribute in the carrier tunnel mechanism. (b) Energy band diagram of M/IL/p^{+2}-SnS tunnel junction under zero, small reverse and large reverse bias condition. E_c, E_g, E_v, and E_f are the conduction band edge, band gap, valence band edge and Fermi level of p^{+2}-SnS, respectively. E_{fm} indicates the Fermi level of metal. All scales are relative only. Under small reverse bias, there exists a direct tunnel path for carrier from metal to p^{+2}-SnS. At larger reverse bias, the trap states existing inside the IL contribute to carrier tunneling and an eventual recombination, leading to a decrease in current (negative resistance).

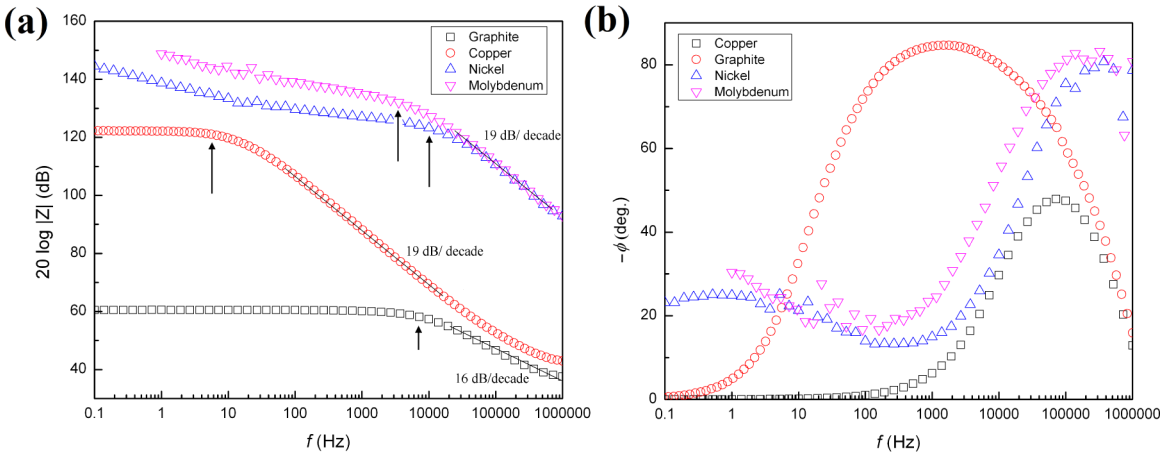

Figure 6. (a) Bode amplitude plots for M/SnS/In_2S_3/F:SnO_2 (M = Copper, Graphite, Nickel, or Molybdenum) devices. Arrows indicate the break points in the impedance plot. Solid lines are the straight line fits in the high frequency linear region of the plots. (b) Bode phase plots for these devices, where a low frequency peak corresponds to the inhomogeneity associated with the interface between the electrode (back contact) and semiconductor (absorber).

Figure 3(c), which in turn has caused larger C_{bc}^{*} as compared to other contacts.

The diffusive signature at low frequencies in the Nyqusit plots corresponding to Ni and Mo as back contact (Figure 2(c),

(d), respectively) indeed required an additional Warburg element, σ in the equivalent circuit of Figure 1(b) to best fit the experimental data. The subsequent circuit model fit shows that R_s was negative in the case of M = Ni and Mo. In order to test its physical validity, the forward bias current−voltage (IV) characteristic of the device for Ni and Mo was measured in the dark and is shown in the inset of Figure 2(b),(c), respectively. It was evident from the IV curves that a negative resistance could exist in these devices. The negative resistance behavior is common in a metal−insulator−semiconductor (MIS) junction when the semiconductor is degenerate or overdoped.[40] In MIS devices, the insulating layer consisting of trap states acts as a tunneling medium for charge carriers. In the present case, both Ni/SnS and Mo/SnS interfaces due to their large INI (nonuniformity) can lead to a large density of trap states. However, a partial diffusion of Ni or Mo in SnS can make the SnS layer degenerate close to the interface. The possibility of formation of NiS or MoS_2 cannot be ruled out as well.[41,42] Therefore, the formation of an interfacial layer (IL) is likely around the Ni/SnS and Mo/SnS interfaces.

Figure 5(a) shows the device structure indicating this "IL", an overdoped region of SnS as p^{+2}-SnS and the biasing schemes of our devices to measure the $I-V$ response. Connection-2 ensures that the p^{+2}-SnS/IL/M junction is reverse biased. Figure 5(b) shows the band diagram across this MIS junction under zero bias, a small reverse bias and larger reverse bias condition. Under small reverse bias, electron from the metal tunnel through the barrier IL to the Fermi level of p^{+2}-SnS. As the reverse bias increases, electrons from metal tunnel through the trap states in IL as well and eventually recombine with holes at the valence band of p^{+2}-SnS, causing a decrease in the net current in the device and hence a negative resistance should appear. This implies in case of Ni and Mo back contacts; electron transfer between the semiconducting layer and metal is not just by direct charge injection but by the tunneling as well.

Figure 6(a),(b) shows a typical Bode amplitude and phase plots, respectively, for the tested devices. The Bode analysis is presented in order to confirm the nature of the inhomogeneities associated with various possible sources, such as defects, grain boundaries, diffusion, etc. As shown in Figure 6(a), the high frequency asymptote of the Bode plot corresponding to the device having Cu, Ni, and Mo as back contact has a slope close to 20 dB/decade, which is a characteristic of a linear time invariant system, whereas for Graphite, it is lower (∼16 dB/decade). The breakpoints in these curves were determined from the corner frequency (ω_c) for which the impedance was lower by −3 dB and are indicated by the arrows in Figure 6(a). The relative position of the corner frequency indicates the origin of nature of inhomogeneity in the system which is complemented by the Bode phase plot in Figure 6(b). A low frequency maximum in the Bode phase plot is originated from the interfaces and diffusion around the metal contact, the high frequency maximum appears from individual grains, and all those peaks appearing intermediate correspond to the grain boundaries.[43,44] In the case of Graphite, Ni, and Mo, the largest contribution to the phase parameter is found to be originated by the grains itself. The low frequency rise of the phase values in Ni and Mo are mainly due to the disorders associated with these interfaces, giving rise to an Warburg impedance, as mentioned above. In case of Cu, the only contributor to the phase plot is the grain boundary, as revealed by a large maximum around f = 5 kHz, and therefore it causes a negligible depletion of charges around the Cu/SnS interface. Figure 7

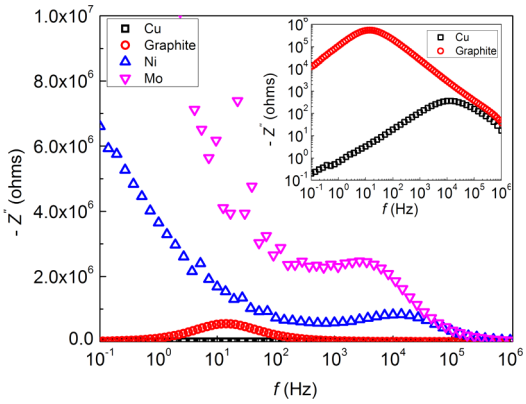

Figure 7. Imaginary impedance plots for M/SnS/In_2S_3/F:SnO_2 (M = Copper, Graphite, Nickel, or Molybdenum) devices. Inset is showing that Copper and Graphite as back contacts offer much smaller loss peaks as compared to Ni or Mo.

shows the imaginary impedance as a function of frequency, which essentially gives a loss spectrum for a given device. The device with Ni and Mo as back contact shows greater loss at lower frequency or the losses occurring around the contacts. In case of Ni, R_c was calculated to be 9.8 MΩ. This large value of R_c has made the curve sharply fall in the frequency range all the way up to 100 kHz, leaving only a negligible contribution of C_c that would have been responsible for the rising branch of this curve. A similar occurrence was noted for Mo as well. On the contrary, Cu and Graphite showed a distinct maximum midway in the frequency range selected. In case of Graphite, the loss is much smaller as compared to Ni or Mo, but should occur around the contacts. For Cu, the loss peak is shifted toward higher frequency, representing the ohmic loss only at the bulk (quasi neutral) region and grain boundaries of SnS. Thus, any significant losses due to contact inhomogeneity should be ruled out when evaporated Cu is used as back contact metal.

CONCLUSIONS

In summary, we have presented a generic strategy of selection of back metal contact in thin film heterojunction solar cells with the help of impedance spectroscopy. Although a proper selection of heterojunction partner for SnS solar cells can reduce the conduction band offset and increase its open circuit voltage, the interface inhomogeneities and nonideal nature largely associated with the back contact induces poor fill factor in the device. The problem is severe in the case of the SnS absorber layer is grown by nonvacuum technique. Four possible back metals, Cu, Graphite, Ni, and Mo, on the basis of their work function suitability were chosen in the case of spray deposited SnS/In_2S_3 heterojunction solar cells. Back metals Ni and Mo were found unsuitable for this device due to the incorporation of large inhomogeneities around the interface and causing a tunneling assisted recombination. It causes both the incorporation of large series resistance and lowering of shunt resistance of the device, which in turn lowers their fill factor. However, graphite contact was more ideal in terms of contact homogeneity and lower series resistance. However, it showed a small depletion of charge, unsuitable for its mechanical instability. Thermally evaporated Cu was demonstrated to have least charge depletion around Cu/SnS interface, good homogeneities and smallest contact resistance as compared to other tested metals, making it a suitable ohmic contact selection for SnS solar cells.

■ ASSOCIATED CONTENT

Supporting Information

(1) The structural and optical properties of SnS and In_2S_3; (2) the illuminated $J-V$ characteristics of SnS solar cell having a Cu back contact; (3) the photoelectrochemical cell response of developed SnS material; (4) the energy dispersive X-ray studies for Cu/SnS interface; (5) the photograph of produced batch of SnS solar cell; and (6) dark $J-V$ characteristics of SnS solar cell with various possible back contacts. This material is available free of charge via the Internet at http://pubs.acs.org/.

■ AUTHOR INFORMATION

Corresponding Author

*Phone: +91 79 23275304. Fax: +91 79 23275030. E-mail: abhijit.ray1974@gmail.com.

Notes

The authors declare no competing financial interest.

■ ACKNOWLEDGMENTS

This work was supported by the PDPU internal grant. The authors thank the Solar Research and Development Center (SRDC, PDPU) for providing XRD and FE-SEM facilities. Prof. Indrajit Mukhopadhyay, Head, SRDC is gratefully acknowledged for providing valuable feedback. Graduate students Mr. Dipal Patel and Ms. Khusbu Chauhan are being acknowledged for their kind support in the impedance measurement. Defence Research and Development Organization (DRDO), New Delhi is being acknowledged for the use of Solar Simulator under Project No. ERIP/ER/1103946/M/01/1349. Department of Science and Technology (DST), New Delhi is acknowledged for the potentiostat-galvanostat facility under Project No. SR/S1/PC-44/2011. Mr. Pranay Soni, Sr. Research Engineer (Machine Vision), Jekson Vision Pvt. Ltd. is gratefully acknowledged for providing valuable feedback on FESEM image analysis.

■ REFERENCES

(1) Sinsermsuksakul, P.; Hartman, K.; Kim, S. B.; Heo, J.; Sun, L.; Park, H. H.; Chakraborty, R.; Buonassisi, T.; Gordon, R. G. Enhancing The Efficiency of SnS Solar Cells Via Band-Offset Engineering with A Zinc Oxysulfide Buffer Layer. *Appl. Phys. Lett.* **2013**, *102*, 053901.

(2) Patel, M.; Mukhopadhyay, I.; Ray, A. Annealing Influence Over Structural and Optical Properties of Sprayed SnS Thin Films. *Opt. Mater.* **2013**, *35*, 1693−1699.

(3) Ramakrishna Reddy, K.; Koteswara Reddy, N.; Miles, R. Photovoltaic Properties of SnS Based Solar Cells. *Sol. Energy Mater. Sol. Cells* **2006**, *90*, 3041−3046.

(4) Sajeesh, T.; Warrier, A. R.; Kartha, C. S.; Vijayakumar, K. Optimization of Parameters of Chemical Spray Pyrolysis Technique to Get n and p-type Layers of SnS. *Thin Solid Films* **2010**, *518*, 4370−4374.

(5) Lopez, S.; Ortiz, A. Spray Pyrolysis Deposition of Sn_xS_y Thin Films. *Semicond. Sci. Technol.* **1994**, *9*, 2130.

(6) Steichen, M.; Djemour, R.; Gultay, L.; Guillot, J.; Siebentritt, S.; Dale, P. J. Direct Synthesis of Single-Phase p-Type SnS by Electrodeposition from a Dicyanamide Ionic Liquid at High Temperature for Thin Film Solar Cells. *J. Phys. Chem. C* **2013**, *117*, 4383−4393.

(7) Ikuno, T.; Suzuki, R.; Kitazumi, K.; Takahashi, N.; Kato, N.; Higuchi, K. SnS Thin Film Solar Cells with $Zn_{1-x}Mg_xO$ Buffer Layers. *Appl. Phys. Lett.* **2013**, *102*, 193901.

(8) Manohari, A. G.; Dhanapandian, S.; Manoharan, C.; Kumar, K. S.; Mahalingam, T. Effect of Doping Concentration on The Properties of Bismuth Doped Tin Sulfide Thin Films Prepared by Spray Pyrolysis. *Mater. Sci. Semicond. Process.* **2014**, *17*, 138−142.

(9) Wang, Z.; Qu, S.; Zeng, X.; Liu, J.; Tan, F.; Bi, Y.; Wang, Z. Organic/Inorganic Hybrid Solar Cells Based on SnS/SnO Nanocrystals and MDMO-PPV. *Acta Mater.* **2010**, *58*, 4950−4955.

(10) Wang, Z.; Qu, S.; Zeng, X.; Liu, J.; Zhang, C.; Tan, F.; Jin, L.; Wang, Z. The Application of SnS Nanoparticles to Bulk Heterojunction Solar Cells. *J. Alloys Compd.* **2009**, *482*, 203−207.

(11) Ogah, O. E.; Reddy, K. R.; Zoppi, G.; Forbes, I.; Miles, R. W. Annealing Studies and Electrical Properties of SnS-based Solar Cells. *Thin Solid Films* **2011**, *519*, 7425−7428.

(12) Abou-Elfotouh, F. A.; Kazmerski, L.; Moutinho, H.; Wissel, J.; Dhere, R.; Nelson, A.; Bakry, A. Determination and Observation of Electronic Defect Levels in $CuInSe_2$ Crystals and Thin Films. *J. Vac. Sci. Technol., A* **1991**, *9*, 554−558.

(13) Igalson, M.; Schock, H. The Metastable Changes of The Trap Spectra of $CuInSe_2$-based Photovoltaic Devices. *J. Appl. Phys.* **1996**, *80*, 5765−5769.

(14) Igalson, M.; Platzer-Borkman, C. The Influence of Buffer Layer on The Transient Behavior of Thin Film Chalcopyrite Devices. *Sol. Energy Mater. Sol. Cells* **2004**, *84*, 93−103.

(15) Walter, T.; Herberholz, R.; Müller, C.; Schock, H. Determination of Defect Distributions from Admittance Measurements and Application to $Cu(In,Ga)Se_2$ Based Heterojunctions. *J. Appl. Phys.* **1996**, *80*, 4411−4420.

(16) Hanna, G.; Jasenek, A.; Rau, U.; Schock, H. Influence of The Ga-content on The Bulk Defect Densities of $Cu(In,Ga)Se_2$. *Thin Solid Films* **2001**, *387*, 71−73 Proceeedings of Symposium N on Thin Film Photovoltaicmaterials of the E-MRS Spring Conference.

(17) Turcu, M.; Rau, U. Compositional Trends of Defect Energies, Band Alignments, and Recombination Mechanisms in The $Cu(In,Ga)(Se,S)_2$ alloy system. *Thin Solid Films* **2003**, *431*, 158−162.

(18) Lee, J.; Cohen, J. D.; Shafarman, W. N. The Determination of Carrier Mobilities in CIGA Photovoltaic Devices using High-Frequency Admittance Measurements. *Thin Solid Films* **2005**, *480*, 336−340.

(19) Sakurai, T.; Ishida, N.; Ishizuka, S.; Islam, M.; Kasai, A.; Matsubara, K.; Sakurai, K.; Yamada, A.; Akimoto, K.; Niki, S. Effects of Annealing Under Various Atmospheres on Electrical Properties of $Cu(In,Ga)Se_2$ Films and $CdS/Cu(In,Ga)Se_2$ Heterostructures. *Thin Solid Films* **2008**, *516*, 7036−7040.

(20) Logan, B. E.; Hamelers, B.; Rozendal, R.; Schröder, U.; Keller, J.; Freguia, S.; Aelterman, P.; Verstraete, W.; Rabaey, K. Microbial Fuel Cells: Methodology and Technology. *Environ. Sci. Technol.* **2006**, *40*, 5181−5192.

(21) Jüttner, K. Electrochemical Impedance Spectroscopy (EIS) of Corrosion Processes on Inhomogeneous Surfaces. *Electrochim. Acta* **1990**, *35*, 1501−1508.

(22) Wang, Q.; Moser, J.-E.; Grätzel, M. Electrochemical Impedance Spectroscopic Analysis of Dye-Sensitized Solar Cells. *J. Phys. Chem. B* **2005**, *109*, 14945−14953.

(23) Fabregat-Santiago, F.; Garcia-Belmonte, G.; Mora-Sero, I.; Bisquert, J. Characterization of Nanostructured Hybrid and Organic Solar Cells by Impedance Spectroscopy. *Phys. Chem. Chem. Phys.* **2011**, *13*, 9083−9118.

(24) Kumar, S.; Singh, P.; Chilana, G. Study of Silicon Solar Cell at Different Intensities of Illumination and Wavelengths Using Impedance Spectroscopy. *Sol. Energy Mater. Sol. Cells* **2009**, *93*, 1881−1884.

(25) Proskuryakov, Y. Y.; Durose, K.; Taele, B. M.; Oelting, S. Impedance Spectroscopy of Unetched CdTe/CdS Solar Cells—Equivalent Circuit Analysis. *J. Appl. Phys.* **2007**, *102*, 024504.

(26) Fernandes, P. A.; Sartori, A. F.; Salomé, P. M. P.; Malaquias, J.; da Cunha, A. F.; Graça, M. P. F.; González, J. C. Admittance Spectroscopy of Cu_2ZnSnS_4 Based Thin Film Solar Cells. *Appl. Phys. Lett.* **2012**, *100*, 233504.

(27) Bisquert, J.; Vikhrenko, V. S. Interpretation of The Time Constants Measured by Kinetic Techniques in Nanostructured Semiconductor Electrodes and Dye-Sensitized Solar Cells. *J. Phys. Chem. B* **2004**, *108*, 2313−2322.

(28) Ye, H.; Park, H. S.; Akhavan, V. A.; Goodfellow, B. W.; Panthani, M. G.; Korgel, B. A.; Bard, A. J. Photoelectrochemical Characterization of $CuInSe_2$ and $Cu(In_{1-x}Ga_x)Se_2$ Thin Films for Solar Cells. *J. Phys. Chem. C* **2010**, *115*, 234−240.
(29) Bayhan, H.; Kavasoğlu, A. S. Study of $CdS/Cu(In,Ga)Se_2$ Heterojunction Interface Using Admittance and Impedance Spectroscopy. *Sol. Energy* **2006**, *80*, 1160−1164.
(30) Sugiyama, M.; Hayashi, M.; Yamazaki, C.; Hamidon, N. B.; Hirose, Y.; Itagaki, M. Application of Impedance Spectroscopy to Investigate the Electrical Properties Around The *pn* Interface of $Cu(In,Ga)Se_2$ Solar Cells. *Thin Solid Films* **2013**, *535*, 287−290.
(31) Schneikart, A.; Schimper, H.; Klein, A.; Jaegermann, W. Efficiency Limitations of Thermally Evaporated Thin-film SnS Solar Cells. *J. Phys. D: Appl. Phys.* **2013**, *46*, 305109.
(32) Britt, J.; Ferekides, C. Thin-film CdS/CdTe Solar Cell With 15.8% Efficiency. *Appl. Phys. Lett.* **1993**, *62*, 2851−2852.
(33) Macdonald, J.; Kenan, W. *Impedance Spectroscopy: Emphasizing Solid Materials and Systems*; Wiley Interscience: New York, 1987.
(34) Cole, K. S.; Cole, R. H. Dispersion and Absorption in Dielectrics I. Alternating Current Characteristics. *J. Chem. Phys.* **1941**, *9*, 341−351.
(35) Córdoba-Torres, P.; Mesquita, T.; Devos, O.; Tribollet, B.; Roche, V.; Nogueira, R. On The Intrinsic Coupling Between Constant-Phase Element Parameters α and Q in Electrochemical Impedance Spectroscopy. *Electrochim. Acta* **2012**, *72*, 172−178.
(36) Schroder, D. *Semiconductor Materials and Device Characterizations*, 3rd ed.; Wiley: New York, 2006.
(37) Proskuryakov, Y. Y.; Durose, K.; Turkestani, M. K. A.; Mora-Seró, I.; Garcia-Belmonte, G.; Fabregat-Santiago, F.; Bisquert, J.; Barrioz, V.; Lamb, D.; Irvine, S. J. C.; Jones, E. W. Impedance Spectroscopy of Thin-Film CdTe/CdS Solar Cells Under Varied Illumination. *J. Appl. Phys.* **2009**, *106*, 044507.
(38) Garcia-Belmonte, G.; Garca-Caadas, J.; MoraSer, I.; Bisquert, J.; Voz, C.; Puigdollers, J.; Alcubilla, R. Effect of Buffer Layer on Minority Carrier Lifetime and Series Resistance of Bifacial Heterojunction Silicon Solar Cells Analyzed by Impedance Spectroscopy. *Thin Solid Films* **2006**, *514*, 254−257.
(39) Boix, P. P.; Ajuria, J.; Pacios, R.; Garcia-Belmonte, G. Carrier Recombination Losses in Inverted Polymer: Fullerene Solar Cells with ZnO Hole-Blocking Layer from Transient Photovoltage and Impedance Spectroscopy Techniques. *J. Appl. Phys.* **2011**, *109*, 074514.
(40) Sze, S. M.; Ng, K. K. *Physics of Semiconductor Devices*; John Wiley & Sons: New York, 2006.
(41) Scheer, R.; Lewerenz, H.-J. Formation of Secondary Phases in Evaporated $CuInS_2$ Thin Films: A Surface Analytical Study. *J. Vac. Sci. Technol., A* **1995**, *13*, 1924−1929.
(42) Scragg, J. J.; Wáltjen, J. T.; Edoff, M.; Ericson, T.; Kubart, T.; Platzer-Bjolrkman, C. A Detrimental Reaction at The Molybdenum Back Contact in $Cu_2ZnSn(S,Se)_4$ Thin-Film Solar Cells. *J. Am. Chem. Soc.* **2012**, *134*, 19330−19333.
(43) Sen, S.; Pramanik, P.; Choudhary, R. Impedance Spectroscopy Study of The Nanocrystalline Ferroelectric $(PbMg)(ZrTi)O_3$ System. *Appl. Phys. A: Mater. Sci. Process.* **2006**, *82*, 549−557.
(44) Gao, H.; Yue, Z.; Li, L. Influence of Thickness on The Electrical Properties of $BaTiO_3$ Films Deposited on Ni Substrates by Radio-Frequency Magnetron Sputtering. *J. Phys. D: Appl. Phys.* **2013**, *46*, 045307.